Axonal transport deficits and degeneration can evolve independently in mouse models of amyotrophic lateral sclerosis

Petar Marinković[a], Miriam S. Reuter[a], Monika S. Brill[a], Leanne Godinho[a], Martin Kerschensteiner[b,1,2], and Thomas Misgeld[a,c,d,1,2]

[a]Biomolecular Sensors and Center for Integrated Protein Sciences (Munich) at the Institute of Neuroscience, Technische Universität München, 80802 Munich, Germany; [b]Research Unit Therapy Development, Institute of Clinical Neuroimmunology, Ludwig-Maximilians-Universität München, 81377 Munich, Germany; [c]Institute for Advanced Study, Technische Universität München, 85748 Garching, Germany; and [d]German Center for Neurodegenerative Diseases (DZNE), 80336 Munich, Germany

Edited* by Joshua R. Sanes, Harvard University, Cambridge, MA, and approved January 31, 2012 (received for review January 13, 2012)

Axonal transport deficits have been reported in many neurodegenerative conditions and are widely assumed to be an immediate causative step of axon and synapse loss. By imaging changes in axonal morphology and organelle transport over time in several animal models of amyotrophic lateral sclerosis (ALS), we now find that deficits in axonal transport of organelles (mitochondria, endosomes) and axon degeneration can evolve independently. This conclusion rests on the following results: (*i*) Axons can survive despite long-lasting transport deficits: In the SOD^{G93A} model of ALS, transport deficits are detected soon after birth, months before the onset of axon degeneration. (*ii*) Transport deficits are not necessary for axon degeneration: In the SOD^{G85R} model of ALS, motor axons degenerate, but transport is unaffected. (*iii*) Axon transport deficits are not sufficient to cause immediate degeneration: In mice that overexpress wild-type superoxide dismutase-1 (SOD^{WT}), axons show chronic transport deficits, but survive. These data suggest that disturbances of organelle transport are not a necessary step in the emergence of motor neuron degeneration.

neuromuscular junction | time-lapse imaging

Neurons use axonal transport to shuttle organelles and vesicles essential for their function and survival between soma and synapses (1, 2). It thus appears logical that intact axonal transport is an important requirement for neuronal survival. Consistent with this idea, it has been shown that mutations in transport-related genes can result in neurodegenerative phenotypes in mice and humans (3, 4). Because transport deficits have been reported in many neurodegenerative diseases, including Alzheimer's disease, Huntington's disease, and amyotrophic lateral sclerosis (ALS) (5–8), it is commonly assumed that disturbances in axonal transport are key pathological events that contribute to neurodegeneration (9–11). However, the causal relationship of axonal transport disturbances to degeneration remains unclear. This disconnect is at least partially due to the fact that it has been difficult to directly monitor axonal transport in living tissue at the single axon level.

Here, we use a recently developed imaging approach based on the transgenic labeling of mitochondria (12) to assay the evolution of organelle transport deficits and their possible consequences, such as axon degeneration, target denervation, and motor impairment, in several animal models of the neurodegenerative disease, ALS. We chose ALS models to study the relation between axonal transport deficits and degeneration for a number of reasons. First, several suitable and well-characterized animal models are available, which are based on human SOD mutations found in familial ALS patients (SOD^{G93A}, ref. 13; SOD^{G37R}, ref. 14; SOD^{G85R}, ref. 15). Second, ALS primarily affects motor neurons, which are among the largest neurons in the body and should therefore be particularly vulnerable to transport deficits. Finally, abnormalities of organelle transport in ALS animal models (7, 8, 16), and even in humans suffering from ALS (17), are well documented in vitro and in vivo.

Surprisingly, our results reveal that axonal transport deficits and degeneration can be dissociated in SOD-based ALS models. Although transport deficits precede axon degeneration in the most commonly used SOD^{G93A} and SOD^{G37R} models, no transport deficits were found in the SOD^{G85R} model despite ongoing axon degeneration. Conversely, transport deficits occur in the absence of degeneration in SOD^{WT} mice that overexpress wild-type SOD. Taken together, these findings indicate that transport deficits are neither necessary nor sufficient to cause axon degeneration in these classical ALS models.

Results

Axonal Transport Deficits Long Precede Axon Degeneration in SOD^{G93A} Mice. We first investigated the most commonly used animal model of ALS, the SOD^{G93A} mouse (13). In this model, mutant mice start to develop clinical symptoms (weight loss followed by weakness) around 3–4 mo of age (Fig. 1*A*). During the same time period, denervation of neuromuscular junctions (NMJs) becomes obvious in various muscles, including the triangularis sterni and gastrocnemius (Fig. 1*B*). To analyze the transport and distribution of mitochondria, a major anterograde and retrograde transport cargo, we crossed SOD^{G93A} mice with *Thy1-MitoCFP* mice, which selectively express cyan fluorescent protein (CFP) in neuronal mitochondria (12). Consistent with reduced mitochondrial transport, SOD^{G93A}, *Thy1-MitoCFP* double-transgenic mice showed a reduced density of mitochondria in motor axons and NMJs in the triangularis sterni, but not in ALS-resistant sensory axons in the saphenous nerve (Fig. S1 *A* and *B*). Similar changes were observed in NMJs in the gastrocnemius muscle ($35.7 \pm 1.3\%$ mitochondrial coverage in control mice vs. 18.8 ± 1.0 in SOD^{G93A} mice; mean ± SEM; $P < 0.05$). To investigate whether the reduction of mitochondrial density is a consequence of reduced transport, we directly measured the flux of fluorescently labeled mitochondria in intercostal nerves in triangularis sterni nerve-muscle explants (18) and in isolated tibialis nerves (the nerve that innervates the gastrocnemius muscle; ref. 19). Indeed, in both

Author contributions: M.K. and T.M. designed research; P.M., M.S.R., and M.S.B. performed research; L.G. contributed new reagents/analytic tools; P.M., M.S.R., and M.S.B. analyzed data; and P.M., L.G., M.K., and T.M. wrote the paper.

The authors declare no conflict of interest.

*This Direct Submission article had a prearranged editor.

Freely available online through the PNAS open access option.

[1]M.K. and T.M. contributed equally to this work.

[2]To whom correspondence may be addressed. E-mail: thomas.misgeld@lrz.tum.de or martin.kerschensteiner@med.uni-muenchen.de.

This article contains supporting information online at www.pnas.org/lookup/suppl/doi:10.1073/pnas.1200658109/-/DCSupplemental.

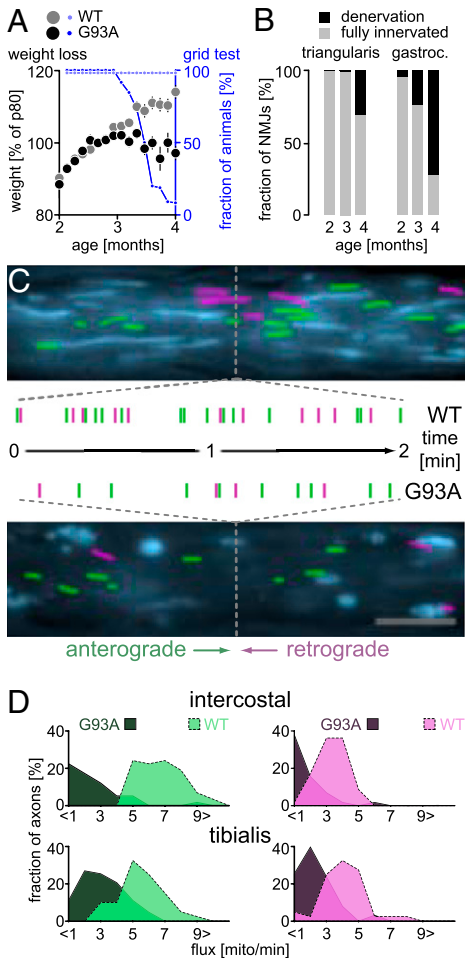

Fig. 1. Axonal transport deficits are observed in *SOD*^{G93A} mice. (*A*) Time-course of body weight (% of weight at P80, mean ± SEM) and grid test performance (% of mice with normal test; $n \geq 10$ mice per group). (*B*) Time-course of denervation in triangularis sterni and gastrocnemius muscles (>1,500 synapses, $n \geq 5$ mice). (*C*) Wide-field images of intercostal axons (average of 50 frames). Stationary mitochondria, cyan. Moving mitochondria (from first, 25th, and 50th frames of the movie) are indicated as pseudo-colored overlays. In *Middle*, an "event" diagram is shown, where all time-points when moving mitochondria crossed the indicated line over a 2-min period are shown as vertical color-coded marks (green, anterograde; magenta, retrograde). (*D*) Frequency distribution of mitochondrial flux in axons of intercostal (*Upper*) and tibialis nerves (*Lower*; $n > 40$ axons, $n \geq 4$ mice) at 4 mo of age. (Scale bar: 5 μm.)

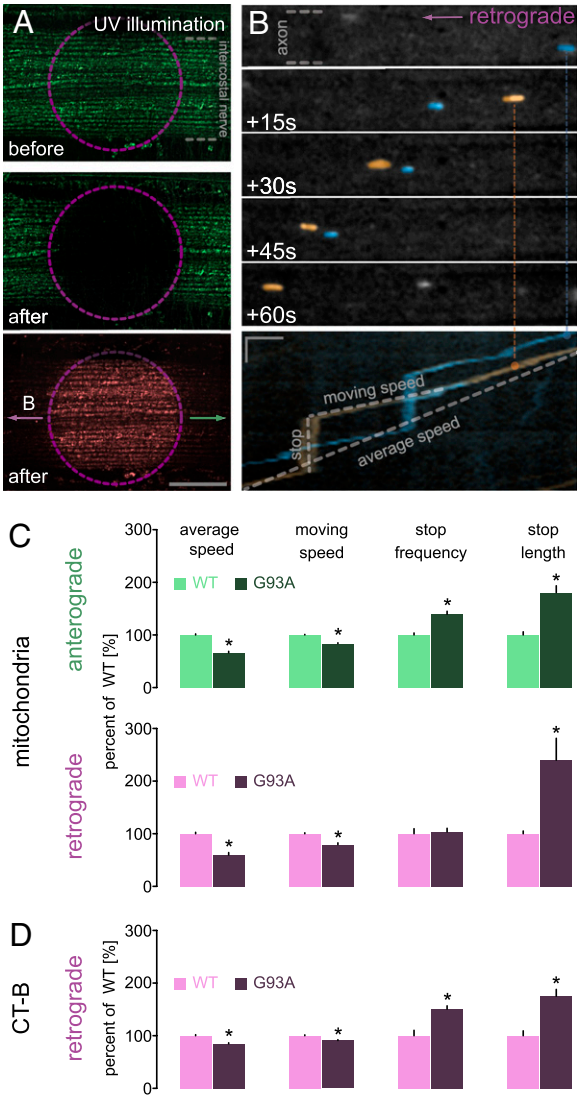

Fig. 2. Reduced speed and increased stop length of mitochondria and vesicles in *SOD*^{G93A} mice. (*A*) Intercostal nerve in a *Thy1-MitoKaede* mouse before (*Top*, green channel) and after (*Middle*, green channel; *Bottom*, red channel) localized photoconversion (UV-exposed area outlined in magenta). (*B Upper*) Time-lapse images of photoconverted mitochondria (pseudocolored blue and brown). (*B Lower*) Corresponding kymograph. (*C*) Single-cargo transport characteristics of individual mitochondria (n = 195–386 mitochondria; $n \geq 29$ axons; n = 4 mice) at 4 mo of age. (*D*) Single-cargo transport characteristics of individual CTB-labeled vesicles (n = 384–386 vesicles; $n \geq 24$ axons; n = 4 mice) at 4 mo of age. Values are expressed as mean percentage ± SEM of WT control in *C* and *D*. (Scale bars: *A*, 100 μm; *B*, *y* axis, 10 s; *B*, *x* axis, 10 μm.) *$P < 0.001$.

preparations, anterograde and retrograde transport flux of mitochondria were reduced in *SOD*^{G93A}, *Thy1-MitoCFP* motor axons at an advanced stage of the disease (4 mo after birth; Fig. 1 *C* and *D* and Movie S1).

We extended these results with two sets of experiments. First, to better understand the changes in mitochondrial motility underlying the transport deficits in *SOD*^{G93A} mice, we established an approach that allows single cargo analysis in motor axons in situ. We generated transgenic mice, which express the photoconvertible fluorescent protein, Kaede (20), selectively in neuronal mitochondria (*Thy1-MitoKaede* mice). We then photoconverted a spatially restricted population of mitochondria from green to red fluorescence by using 405-nm illumination (Fig. 2*A*). By imaging the axons either distal or proximal to the site of photoconversion, we could track the anterograde or retrograde movement of individual red mitochondria amid their non-photoconverted green counterparts (Fig. 2*B* and Movie S2). This single cargo analysis revealed a reduction in average mitochondrial speed in *SOD*^{G93A} mice that is characterized by pronounced changes in stop length and frequency (Fig. 2*C*). Second, we asked whether these defects are specific to mitochondria by investigating transport of another cargo. For this purpose, we injected Cholera Toxin Subunit B (CTB) conjugated to Alexa Fluor 594 into the triangularis sterni muscle in vivo (21). The CTB–dye complex is taken up by neuromuscular synapses and incorporated into vesicles, likely of endosomal nature (22), which are then transported retrogradely to the cell body. By imaging intercostal axons 24 h after injection, we found that transport of CTB-labeled vesicles was affected in a similar manner as mitochondrial transport (Fig. 2*D* and Movie S3).

We next wanted to understand when during the disease course transport deficits emerged. To do so, we measured mitochondrial flux in SOD^{G93A} mice between 10 d and 4 mo after birth. Deficits were detectable as early as postnatal day (P)20 for anterograde transport and P40 for retrograde transport (Fig. 3), long preceding the drop in mitochondrial density (Fig. S1*C*). The emergence of deficits in anterograde transport before retrograde transport conforms to previous results obtained in cell culture, where anterograde transport was affected more (7). Further, to confirm that the transport deficits found in SOD^{G93A} mice are not due to the insertion site of the transgene, we compared them to a very similar model of ALS, SOD^{G37R} mice (14). Also in this model, transport deficits were evident at presymptomatic stages (2 mo of age; Fig. 3). To assess whether transport deficits were specific for motor axons, as would be expected for the motor neuron disease ALS, we examined the purely sensory saphenous nerve. Indeed, here transport flux was normal even in late-stage SOD^{G93A} mice (4 mo of age; "saph." in Fig. 3).

Finally, because transport deficits are present long before the first clinical signs of the disease become manifest, we wanted to examine how such long-lasting transport deficits would affect the distal arbors of motor neurons, a site that is likely most susceptible to a long-standing reduction in organelle supply. To address this question, we took advantage of *Thy1-YFP*^{H} mice that, because of labeling of small numbers of motor neurons, permit reconstructions of entire motor units (23, 24). We first measured mitochondrial flux in axons, which were fluorescently labeled with cytoplasmic YFP in SOD^{G93A}, *Thy1-MitoCFP*, *Thy1-YFP*^{H} triple-transgenic mice. We then reconstructed the distal arbors of such axons by high-resolution confocal microscopy ($n = 3$). Remarkably, we found that motor neurons with severely compromised transport support arbors that terminate in normal appearing NMJs, although mitochondrial density was already reduced (Fig. S2).

Dissociation of Axonal Transport Deficits from Axon Loss in SOD^{G85R} and SOD^{WT} Mice. That neurons can survive long-term in the presence of severe transport deficits implies that a reduction of organelle transport does not immediately lead to axon degeneration. This disjunction between transport deficits and axon degeneration was confirmed by the analysis of SOD^{G85R} mutant mice (15). These mice start losing weight ≈9 mo after birth (Fig. 4*A*). Subsequently, during the preterminal phase of the disease (for exact ages, see *Materials and Methods*), they also develop muscle weakness (Fig. 4*A*), coincident with denervation of muscle fibers (Fig. 4*B*). Assaying axonal mitochondria in triangularis sterni muscle and tibialis nerve explants from SOD^{G85R}, *Thy1-MitoCFP* mice, however, revealed normal anterograde and retrograde flux, speed, and density, even in the preterminal stage of the disease, when axon fragments were readily detectable in the imaged nerves (Fig. 4 *C* and *D*, Figs. S3 and S4, and Movie S4). Only in the terminal stage of the disease, a few days before the animals die, at a time when many axons in the affected nerves have already degenerated, did we detect a mild drop in anterograde mitochondrial flux (from 5.9 ± 0.3 mitochondria per min in WT to 5.1 ± 0.3 mitochondria per min in SOD^{G85R} mice; mean ± SEM; $P < 0.05$). Similarly, retrograde transport of endosomal vesicles labeled by peripheral injection of CTB showed no abnormalities in intercostal or tibialis nerves (Fig. 4*E* and Fig. S3*C*).

Axons can thus degenerate without preceding transport deficits, but is the converse also true, i.e., are there models in which axonal transport is disrupted while axons survive? Our analysis of SOD^{WT}

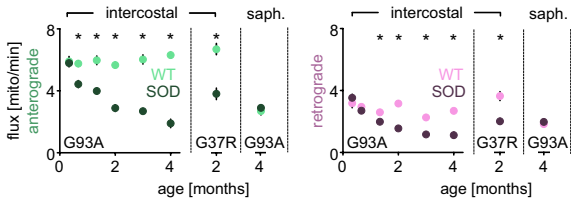

Fig. 3. Axonal transport deficits are observed early in SOD^{G93A} mice. Time-course of anterograde (*Left*) and retrograde (*Right*) mitochondrial flux in intercostal and saphenous ("saph.") nerves of SOD^{G93A} and WT mice ($n > 30$ axons, $n \geq 4$ mice per time-point), and in intercostal nerves of SOD^{G37R} mice ($n = 45$ axons, $n = 2$ mice). The data from SOD^{G93A} intercostal nerves at 4 mo correspond to the data shown as frequency distributions in Fig. 1*D*. Error bars (SEM) are smaller than data symbols in most cases. *$P < 0.001$.

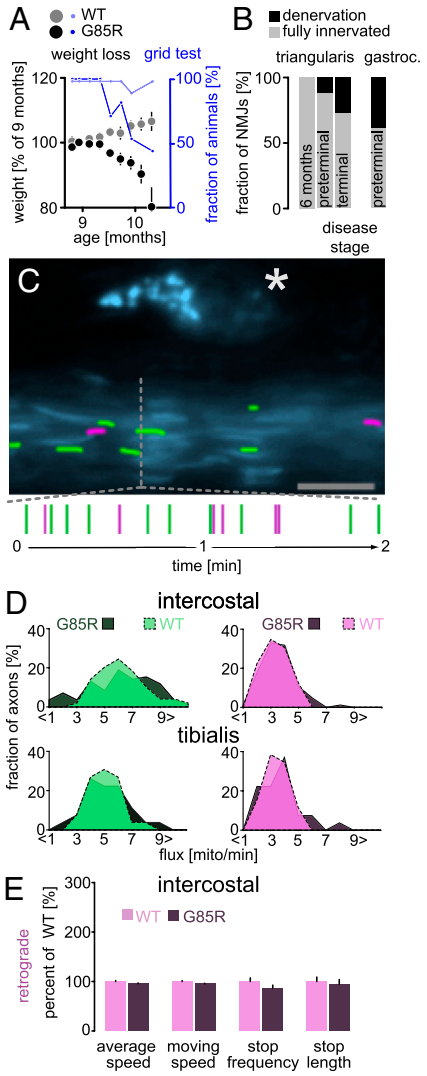

Fig. 4. Axon degeneration but no transport deficits are observed in SOD^{G85R} mice. (*A*) Time-course of body weight (in % of weight at 9 mo of age, mean ± SEM) and grid test performance (expressed as % of mice with normal test; $n \geq 10$ mice per group). (*B*) Denervation in triangularis sterni and gastrocnemius muscles ($n > 250$ synapses, $n > 3$ mice). (*C*) Wide-field image of an intercostal axon presented as described for Fig. 1*C*. Asterisk marks an axonal fragment, commonly found in preterminal SOD^{G85R} mice right next to axons with normal transport. (*D*) Frequency distribution of mitochondrial flux in intercostal and tibialis nerves ($n > 40$ axons, $n \geq 3$ mice) at preterminal stage. (*E*) Single-cargo transport characteristics of individual CTB-labeled vesicles in SOD^{G85R} mice in intercostal nerves at preterminal stage ($n = 300$–304 vesicles; $n = 16$ axons; $n = 3$ mice); Values are expressed as mean percentage ± SEM of WT control. (Scale bar: 5 μm.)

mice suggests that this constellation is possible. SOD^{WT} mice overexpress a nonmutant human SOD protein and are commonly used as control mice in ALS studies (13). As expected, we detected no weight loss, functional deficits, or denervation in these mice when we examined them at 4 mo of age (Fig. 5 *A* and *B*). Surprisingly, however, anterograde and retrograde mitochondrial flux in triangularis sterni explants of SOD^{WT}, *Thy1-MitoCFP* mice was significantly reduced already 2 mo after birth (Fig. S5*A*). This deficit was progressive and reached levels in intercostal and tibialis nerves comparable to SOD^{G93A} and SOD^{G37R} mice by 4 mo and persisted for up to 1 y (Fig. 5 *C* and *D*, Fig. S5, and Movie S5). Mitochondrial density was reduced both in intercostal and tibialis nerves at 4 mo (Fig. S5*B*). Similarly, SOD^{WT} axons showed slowed transport of mitochondria and CTB-labeled particles (Fig. 5*E* and Fig. S4). Thus, overexpression of human nonmutated SOD suffices to induce early transport deficits. These deficits, however, do not cause overt motor neuron degeneration for several months—only at 12 mo did we detect mild denervation (<4% in triangularis; <8% in gastrocnemius muscle; Fig. 5*B*; see also ref. 25).

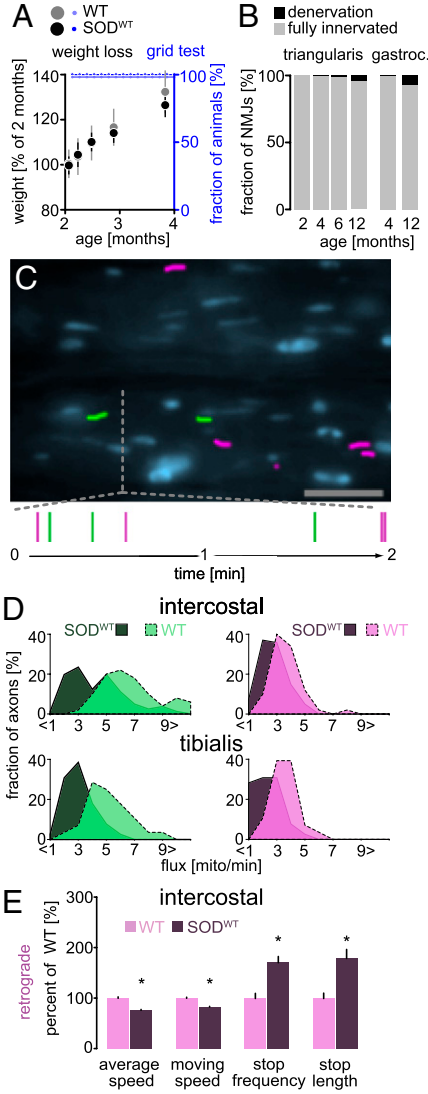

Fig. 5. Axonal transport deficits and degeneration are dissociated in SOD^{WT} mice. (*A*) Time-course of body weight (in % of weight at 2 mo of age, mean ± SEM) and grid test performance (expressed as % of mice with normal test; $n > 10$ mice per group). (*B*) Only minor denervation in triangularis sterni and gastrocnemius muscles is observed in aged SOD^{WT} mice ($n > 250$ synapses, $n > 3$ mice). (*C*) Wide-field image of an intercostal axon presented as described for Fig. 1*C*. (*D*) Frequency distribution of mitochondrial flux in intercostal and tibialis nerves ($n > 40$ axons, $n \geq 3$ mice) at 4 mo of age. (*E*) Single-cargo transport characteristics of individual CTB-labeled vesicles for SOD^{WT} mice in intercostal nerves at 6 mo of age ($n = 120$–280 vesicles; $n = 10$–23 axons; $n = 3$ mice). Values are expressed as mean percentage ± SEM of WT control. (Scale bar: 5 μm.) *$P < 0.001$.

Discussion

The aim of our study was to investigate the in vivo consequences of reduced organelle transport in ALS mice, which—based on the published literature (7, 8, 16, 26, 27)—we expected to be a general feature of ALS disease models. However, when we compared several different bona fide models of SOD-based familial ALS, we found to our surprise that rather than cosegregating with the ALS-specific mutation, transport disturbances were only present in some SOD overexpression models (G93A, G37R, and wild-type SOD, but not G85R), irrespective of whether the enzyme carried an ALS mutation. These results thus dissociate deficits of organelle transport and axon degeneration in animal models of ALS. This conclusion contrasts with widely held assumptions in the field of ALS research, which are based on reduced organelle density in SOD^{G93A} axons (26, 28) and altered organelle motility in SOD^{G93A} axons in vitro (7, 8) and in vivo (16).

One important distinguishing feature of our study is that we performed a systematic time-course comparison of organelle transport in fully mature motor axons in several ALS models that differ in SOD expression level, enzymatic activity, and mutation status. This comparative approach is of importance because it is well-established from human studies that a vast number of different SOD mutations that, for example, differ in their effects on biochemical activity or stability of the enzyme (29), lead to essentially the same ALS phenotype. Any cell biological mechanism that is linked to the root cause of motor neuron degeneration in ALS should therefore probably be similarly affected across the spectrum of disease-related SOD mutations. Our comparison shows that organelle transport disruptions are not directly related to mutation-specific toxicity of SOD, but rather to enzymatic activity, protein expression levels, subcellular localization, or aggregation; however, which combination of these parameters affects transport cannot be definitively differentiated based on our datasets. In contrast to our study, most previous reports on the link between ALS and organelle transport either focused on only one mutation, performed comparisons in vitro or in nonmotor neuron cells, or did not include the wild-type overexpression control SOD^{WT}. Other studies looked at surrogate markers of transport deficits (such as organelle density; refs. 26, 28, and 30). However, organelle density is not a direct indicator of supply by axonal transport, but can be equally affected by catabolic processes (such as autophagy; ref. 31) or local remodelling (such as organelle fusion or fission; ref. 32). It is worth noting that—although this was not the focus of our study—in our material also mitochondrial shape changes were only apparent in SOD^{G93A}, SOD^{G37R}, and SOD^{WT}, but not in SOD^{G85R} mice (compare Fig. 1*C* vs. Fig. 4*C* vs. Fig. 5*C*). Such shape changes are commonly interpreted as evidence of mitochondrial dysfunction or of altered fusion/fission (8), but previous studies in the nondisease-related SOD^{WT} controls have shown that shape changes too can be dissociated from occurrence of an ALS-like disease (25). Indeed, we observed some of the most drastic mitochondrial shape changes in aged SOD^{WT} mice (Fig. 5*C*).

In our view, the fact that SOD^{WT} mice maintain essentially normal neuromuscular innervation despite profound and long-lasting transport deficits that are comparable to those observed in SOD^{G93A} and SOD^{G37R} is a strong argument against the hypothesis that disruptions in organelle transport alone could be the pathogenic mechanism in ALS motor neuron degeneration. Still, previous reports have documented the occurrence of a late-onset form of neurodegeneration in SOD^{WT} mice (25). However, this degeneration does not primarily affect motor neurons, but long

projection neurons of the central nervous system, such as the spino-cerebellar or the dorsal column tracts. In contrast, motor neurons are among the nerve cells that degenerate late, again dissociating this pathology from ALS. Indeed, there is further evidence that argues against a direct role of organelle transport deficits in causing the degenerative phenotype in SOD^{G93A} mice, because increasing mitochondrial transport does not yield the expected therapeutic benefit in SOD^{G93A} mice (33). Furthermore, although the fact that mutations in motor proteins can cause a neurodegenerative phenotype is often cited in support of a role for axonal transport in ALS pathogenesis, mutations in retrograde motor proteins alone do not phenocopy SOD^{G93A} (27). Still, although not primarily pathogenic, the motor axon-specific transport deficits—as seen in SOD^{G93A} or SOD^{G37R} mice—might contribute to the phenotypic variations found between the diseases caused by differentially mutated SOD. Hence, comparing the phenotypes caused by mutations that affect transport and others that do not (such as SOD^{G85R}) might allow differentiating factors that initiate or just accelerate axon degeneration.

A number of general conclusions emerge from our study: First, in ALS models, the mechanisms that reduce organelle transport appear distinct from those that initiate axon degeneration. Hence, axonal transport of organelles might not be a suitable target to therapeutically prevent the irreversible loss of neurons or axons in ALS, although in other neurodegenerative diseases, this might clearly be a promising strategy (34). However, our study does not exclude disturbances in slow axonal transport (35, 36) or changes in cargo composition (27) as important steps in ALS pathogenesis, and does not contradict the view that organelle transport deficits can accelerate axon degeneration, e.g., in the SOD^{G93A} model (25). Moreover, our argument strictly applies only to mitochondria and endosome-derived vesicles. Although these organelles are the most commonly assayed specific cargoes in the context of ALS research, it remains possible that disturbed transport of another cargo would better correlate with ALS-related neurodegeneration. Second, our findings underline the phenotypic heterogeneity that characterizes even closely related animal models of neurodegeneration. This observation emphasizes the need to study several models to differentiate disease-related (e.g., degeneration) from model-related (e.g., transport deficits) events. Third, our study reveals the remarkable capability of motor neurons to survive for long periods of time despite limited axonal transport. Indeed, even in those SOD-overexpression models that affected transport severely, the drop in mitochondrial density was delayed (Fig. 3 vs. Fig. S1*C*), suggesting some compensatory mechanism. One part of this compensation could be the time-shifted drop in retrograde transport, which over time reduces the net deficit in organelle number. This form of compensation would imply a longer residency of individual organelles in the periphery. In the case of mitochondria, an extended lifetime could help to buffer a deficit in the supply of energy substrates. However, in the presence of additional stressors (that might well be ALS-related), the presence of increasingly dysfunctional mitochondria could accelerate axonal demise.

Materials and Methods

Animals. Transgenic mice carrying human wild-type (WT) or mutated SOD1 genes were obtained from Jackson Laboratory. The strains used were the following: SOD^{WT} [Jackson Laboratory strain designation: Tg(SOD1)2Gur/J], SOD^{G93A} (Tg(SOD1*G93A)1Gur/J), SOD^{G37R} (Tg(SOD1*G37R)42Dpr/J), SOD^{G85R} (Tg(SOD1*G85R)148Dwc/J). To study mitochondrial transport, density, and morphology, males from these strains were crossed with *Thy1-MitoCFP*^{C} (Tg(Thy1-CFP/COX8A)C1Lich/J), and—in selected cases—*Thy1-MitoCFP*^{S} (Tg(Thy1-CFP/COX8A)S2Lich/J) or *Thy1-MitoCFP*^{K} females (12) (no differences in transport between strains were found). *Thy1-MitoKaede* mice were generated as described in *SI Materials and Methods* and crossed with SOD mice as indicated above. Double transgenic mice were identified by PCR from tail biopsies. Because *Thy1-MitoCFP* and *Thy1-MitoKaede* animals were maintained on a mixed genetic background, SOD1-negative, MitoCFP- (or MitoKaede-) positive littermates were used as controls. For studying axon morphology and reconstructing motor units, SOD-mutant mice were crossed with *Thy1-YFP*^{16} (Tg(Thy1-YFP)16Jrs/J) and *Thy1-YFP*^{H} (Tg(Thy1-YFPH)2Jrs/J) mice, respectively (37). Genomic copy numbers of the SOD transgene were confirmed by using quantitative PCR as described (38) and yielded the following ΔCT values: SOD^{G85R} 5.8; SOD^{WT} 6.2; SOD^{G93A} 7.1. All animal work conformed to institutional guidelines and was approved by the Animal Study Committee of the Regierung von Oberbayern.

Behavioral Testing. Animals were tested and weighed every 3–4 d. The grid test was a binary modification of a described test (39). Briefly, each mouse was placed onto a metal grid, which was positioned ≈30 cm above a soft surface. The grid was inverted to determine whether an animal could support itself for >30 s. For each animal, three trials were performed with a 5-min rest period in between. The test was scored "normal" if the animal could hold itself for >30 s in at least one trial. In the figures, we show a "survival" curve of the percentage of animals which showed a normal test at a given time.

Staging of SOD^{G85R} Mice. For staging of SOD^{G85R} mice, we deviated from a purely age-based classification, because clinical manifestations at a specific age varied considerably due to the long preclinical period and fast progression once the disease started. We therefore grouped animals by phenotype rather than age. We considered animals that had lost 10% of their peak body weight and showed an abnormal grid test as "preterminal" and used these animals—which would be expected to die within 2–3 wk—as the latest stage that we systematically studied in our experiments. The mean ages of animals in these categories were as follows: preterminal, 302 ± 8 d; terminal, 311 ± 11 d.

Tissue Preparation, Immunohistochemistry, and Confocal Microscopy. Triangularis sterni muscles were fixed after dissection, subsequently processed for immunohistochemistry and analyzed by confocal microscopy as detailed in *SI Materials and Methods*.

Imaging Mitochondrial Transport. Transport of mitochondria was measured as described (12, 18). Briefly, mice were lethally anesthetized with isoflurane and explants of the triangularis sterni muscle were prepared. The anterior thoracic wall (with the attached triangularis sterni muscle and its innervating intercostal nerves) was isolated by cutting the ribs close to the vertebral column. The explant was pinned down on a Sylgard-coated 3.5-cm plastic Petri dish by using minutien pins (Fine Science tools). After excision, explants were kept in 95% O_2/5% CO_2 (vol/vol)-bubbled Ringer's solution (125 mM NaCl, 2.5 mM KCl, 1.25 mM NaH_2PO_4, 26 mM $NaHCO_3$, 2 mM $CaCl_2$, 1 mM $MgCl_2$, and 20 mM Glucose) at all times. During imaging, explants were maintained on a heated stage (33–36 °C) with a slow and steady flow of warmed and oxygenated Ringer's solution. Preparation of triangularis sterni muscles from *Thy1-MitoKaede* mice was done under red light to prevent accidental photoconversion. In addition to intercostal nerves, saphenous and tibialis nerves were studied by using acutely explanted nerves pinned onto a Sylgard-coated 3.5-cm plastic Petri dish. Although the tibialis nerve has a sensory component, we confirmed in control experiments, using selective labeling of motor axons with a transgene the expression of which conditionally depends on a cholinergic marker, choline acetyltransferase (*Chat-cre*, Ai14; obtained from Jackson Laboratory), that the vast majority of the imaged superficial large-caliber axons were motor axons.

Mitochondria were imaged by using an Olympus BX51WI microscope equipped with a 4×/N.A. 0.13 air objective, 20×/N.A. 0.5, and 100×/N.A. 1.0 water-immersion dipping cone objectives, an automated filter wheel (Sutter) and a cooled CCD camera (Retiga EXi; Qimaging) controlled by μManager (an open source microscopy software; ref. 40). Neutral density and infrared-blocking filters in the light path were used to prevent phototoxicity and photobleaching. To follow mitochondrial movement, images were acquired at 1 Hz by using an exposure time of 500 ms for 5 min. Transport characteristics of individual mitochondria were measured in explants from *Thy1-MitoKaede* mice. To highlight individual mitochondria, we exposed intercostal nerves to a short (≈5 s) localized exposure of 405-nm light from an LED light source (Thorlabs) coupled into the microscope's excitation light path. By moving our observation site proximal or distal from the photoconverted spot along the same nerve, we could use the red channel to track individual mitochondria.

Imaging Transport of CTB-Labeled Vesicles. To study transport of endosomal vesicles, CTB conjugated with Alexa Fluor 594 (Invitrogen) was injected into the triangularis sterni muscle by using a micro syringe (Hamilton; ref. 21).

Mice were anesthetized with ketamine-xylazine [KX; 1.5% ketamine and 0.1% (vol/vol) xylazine]. We made two injections of 0.05% (wt/vol) CTB (in 1× PBS) between the second and third, and the third and fourth ribs. The gastrocnemius muscle was labeled in a similar way. We closed the injection site surgically and placed the mice in a heated recovery chamber. Axonal transport of CTB-labeled endosomes was then imaged 24 h after injection in an acute triangularis sterni or tibialis nerve explant preparation as described above.

Image Analysis and Processing. Image analysis was done by using ImageJ/Fiji software. For details, see *SI Materials and Methods*.

ACKNOWLEDGMENTS. We thank Manuela Budak, Yvonne Hufnagel, and Ljiljana Marinković for excellent technical assistance; Rosi Karl and Anna Thomer for generous help; Anne Ladwig for help with control virus injections; Dr. R. W. Burgess (The Jackson Laboratory, Bar Harbor, ME) for providing SOD-transgenic animals; and to Drs. J. Song and J. W. Lichtman (Harvard University) for help with generation of the *Thy1-MitoKaede* mice. T.M. is supported by the Technische Universität München-Institute for Advanced Study, funded by the German Excellence Initiative, Deutsche Forschungsgemeinschaft (DFG) Sonderforschungsbereich SFB 596, the Alexander-von-Humboldt-Foundation, and the Center for Integrated Protein Science (Munich). Work on this project was further supported by the national funding agency ("Bundesministerium für Bildung und Forschung") in the frame of ERA-NET NEURON "iPSoALS" and through a Christopher and Dana Reeve Foundation grant (to T.M.). Work in M.K.'s laboratory is financed through DFG grants (Emmy-Noether Program, SFB 571, and SFB 870), the Federal Ministry of Education and Research (Competence Network Multiple Sclerosis), and the "Verein Therapieforschung für MS-Kranke e.V.". P.M. was supported by the Graduate School of Technische Universität München.

1. Hirokawa N, Niwa S, Tanaka Y (2010) Molecular motors in neurons: Transport mechanisms and roles in brain function, development, and disease. *Neuron* 68: 610–638.
2. Hollenbeck PJ, Saxton WM (2005) The axonal transport of mitochondria. *J Cell Sci* 118: 5411–5419.
3. Puls I, et al. (2003) Mutant dynactin in motor neuron disease. *Nat Genet* 33:455–456.
4. Hafezparast M, et al. (2003) Mutations in dynein link motor neuron degeneration to defects in retrograde transport. *Science* 300:808–812.
5. Stokin GB, et al. (2005) Axonopathy and transport deficits early in the pathogenesis of Alzheimer's disease. *Science* 307:1282–1288.
6. Szebenyi G, et al. (2003) Neuropathogenic forms of huntingtin and androgen receptor inhibit fast axonal transport. *Neuron* 40:41–52.
7. De Vos KJ, et al. (2007) Familial amyotrophic lateral sclerosis-linked SOD1 mutants perturb fast axonal transport to reduce axonal mitochondria content. *Hum Mol Genet* 16:2720–2728.
8. Magrané J, Sahawneh MA, Przedborski S, Estévez AG, Manfredi G (2012) Mitochondrial dynamics and bioenergetic dysfunction is associated with synaptic alterations in mutant SOD1 motor neurons. *J Neurosci* 32:229–242.
9. De Vos KJ, Grierson AJ, Ackerley S, Miller CC (2008) Role of axonal transport in neurodegenerative diseases. *Annu Rev Neurosci* 31:151–173.
10. Bento-Abreu A, Van Damme P, Van Den Bosch L, Robberecht W (2010) The neurobiology of amyotrophic lateral sclerosis. *Eur J Neurosci* 31:2247–2265.
11. Boillée S, Vande Velde C, Cleveland DW (2006) ALS: A disease of motor neurons and their nonneuronal neighbors. *Neuron* 52:39–59.
12. Misgeld T, Kerschensteiner M, Bareyre FM, Burgess RW, Lichtman JW (2007) Imaging axonal transport of mitochondria in vivo. *Nat Methods* 4:559–561.
13. Gurney ME, et al. (1994) Motor neuron degeneration in mice that express a human Cu,Zn superoxide dismutase mutation. *Science* 264:1772–1775.
14. Wong PC, et al. (1995) An adverse property of a familial ALS-linked SOD1 mutation causes motor neuron disease characterized by vacuolar degeneration of mitochondria. *Neuron* 14:1105–1116.
15. Bruijn LI, et al. (1997) ALS-linked SOD1 mutant G85R mediates damage to astrocytes and promotes rapidly progressive disease with SOD1-containing inclusions. *Neuron* 18:327–338.
16. Bilsland LG, et al. (2010) Deficits in axonal transport precede ALS symptoms in vivo. *Proc Natl Acad Sci USA* 107:20523–20528.
17. Breuer AC, et al. (1987) Fast axonal transport in amyotrophic lateral sclerosis: An intra-axonal organelle traffic analysis. *Neurology* 37:738–748.
18. Kerschensteiner M, Reuter MS, Lichtman JW, Misgeld T (2008) Ex vivo imaging of motor axon dynamics in murine triangularis sterni explants. *Nat Protoc* 3:1645–1653.
19. Gilley J, et al. (2011) Age-dependent axonal transport and locomotor changes and tau hypophosphorylation in a "P301L" tau knockin mouse. *Neurobiol Aging* 33:621.e1–621.e15.
20. Ando R, Hama H, Yamamoto-Hino M, Mizuno H, Miyawaki A (2002) An optical marker based on the UV-induced green-to-red photoconversion of a fluorescent protein. *Proc Natl Acad Sci USA* 99:12651–12656.
21. Mantilla CB, Zhan WZ, Sieck GC (2009) Retrograde labeling of phrenic motoneurons by intrapleural injection. *J Neurosci Methods* 182:244–249.
22. Shogomori H, Futerman AH (2001) Cholera toxin is found in detergent-insoluble rafts/domains at the cell surface of hippocampal neurons but is internalized via a raft-independent mechanism. *J Biol Chem* 276:9182–9188.
23. Keller-Peck CR, et al. (2001) Asynchronous synapse elimination in neonatal motor units: Studies using GFP transgenic mice. *Neuron* 31:381–394.
24. Schaefer AM, Sanes JR, Lichtman JW (2005) A compensatory subpopulation of motor neurons in a mouse model of amyotrophic lateral sclerosis. *J Comp Neurol* 490: 209–219.
25. Jaarsma D, et al. (2000) Human Cu/Zn superoxide dismutase (SOD1) overexpression in mice causes mitochondrial vacuolization, axonal degeneration, and premature motoneuron death and accelerates motoneuron disease in mice expressing a familial amyotrophic lateral sclerosis mutant SOD1. *Neurobiol Dis* 7(6 Pt B):623–643.
26. Vande Velde C, et al. (2011) Misfolded SOD1 associated with motor neuron mitochondria alters mitochondrial shape and distribution prior to clinical onset. *PLoS ONE* 6:e22031.
27. Perlson E, et al. (2009) A switch in retrograde signaling from survival to stress in rapid-onset neurodegeneration. *J Neurosci* 29:9903–9917.
28. Pun S, Santos AF, Saxena S, Xu L, Caroni P (2006) Selective vulnerability and pruning of phasic motoneuron axons in motoneuron disease alleviated by CNTF. *Nat Neurosci* 9:408–419.
29. Dion PA, Daoud H, Rouleau GA (2009) Genetics of motor neuron disorders: New insights into pathogenic mechanisms. *Nat Rev Genet* 10:769–782.
30. Shan X, Chiang PM, Price DL, Wong PC (2010) Altered distributions of Gemini of coiled bodies and mitochondria in motor neurons of TDP-43 transgenic mice. *Proc Natl Acad Sci USA* 107:16325–16330.
31. Batlevi Y, La Spada AR (2011) Mitochondrial autophagy in neural function, neurodegenerative disease, neuron cell death, and aging. *Neurobiol Dis* 43:46–51.
32. Detmer SA, Chan DC (2007) Functions and dysfunctions of mitochondrial dynamics. *Nat Rev Mol Cell Biol* 8:870–879.
33. Zhu YB, Sheng ZH (2011) Increased axonal mitochondrial mobility does not slow ALS-like disease in mutant SOD1 mice. *J Biol Chem* 286:23432–23440.
34. d'Ydewalle C, et al. (2011) HDAC6 inhibitors reverse axonal loss in a mouse model of mutant HSPB1-induced Charcot-Marie-Tooth disease. *Nat Med* 17:968–974.
35. Collard JF, Côté F, Julien JP (1995) Defective axonal transport in a transgenic mouse model of amyotrophic lateral sclerosis. *Nature* 375:61–64.
36. Williamson TL, Cleveland DW (1999) Slowing of axonal transport is a very early event in the toxicity of ALS-linked SOD1 mutants to motor neurons. *Nat Neurosci* 2:50–56.
37. Feng G, et al. (2000) Imaging neuronal subsets in transgenic mice expressing multiple spectral variants of GFP. *Neuron* 28:41–51.
38. Alexander GM, et al. (2004) Effect of transgene copy number on survival in the G93A SOD1 transgenic mouse model of ALS. *Brain Res Mol Brain Res* 130:7–15.
39. Kraemer BC, et al. (2010) Loss of murine TDP-43 disrupts motor function and plays an essential role in embryogenesis. *Acta Neuropathol* 119:409–419.
40. Edelstein A, Amodaj N, Hoover K, Vale R, Stuurman N (2010) Computer control of microscopes using microManager. *Curr Protoc Mol Biol* 14:14.